Eur. Phys. J. D (2010)
DOI: 10.1140/epjd/e2010-00215-4

THE EUROPEAN PHYSICAL JOURNAL D

Regular Article

Synchronization regions of two pulse-coupled electronic piecewise linear oscillators

N. Rubido[1], C. Cabeza[1], S. Kahan[1], G.M. Ramírez Ávila[2,3], and Arturo C. Marti[1,a]

[1] Instituto de Física, Universidad de la República, Igua 4225, 11400 Montevideo, Uruguay
[2] Institut für Physik, Humboldt Universität zu Berlin, Germany
[3] Instituto de Investigaciones Físicas, Universidad de San Andrés, La Paz, Bolivia

Received 16 May 2010/ Received in final form 30 June 2010
Published online 30 August 2010 –

Abstract. Stable synchronous states of different order were analytically, numerically and experimentally characterized in pulse-coupled light-controlled oscillators (LCOs). The Master-Slave (MS) configuration was studied in conditions where different time-scale parameters were tuned under varying coupling strength. Arnold tongues calculated analytically – based on the piecewise two-time-scale model for LCOs – and obtained numerically were consistent with experimental results. The analysis of the stability pattern and tongue shape for $(1 : n)$ synchronization was based on the construction of return maps representing the Slave LCO evolution induced by the action of the Master LCO. The analysis of these maps showed that both tongue shape and stability pattern remained invariant. Considering the wide variation range of LCO parameters, the obtained results could have further applications on ethological models.

1 Introduction

Synchronization is a common feature of oscillatory systems and might be understood as an adjustment of rhythms of self-sustained oscillators due to weak interactions [1]. It constitutes an ubiquitous phenomenon and nowadays is a widely spread topic which several books have been devoted to, both from rigorous [2–4] to popularization point of view [5]. Synchronization phenomena are manifested in systems of different nature, ranging from physical [6,7], to chemical [8–10], to biological [11–14] to electronic oscillators [15–19]. The construction of coupled maps has enabled the study of synchronization in different systems, leading to important results, in particular, in the field of neuron dynamics [20,21].

Synchronous regimes of different order [2,3] occur in coupled oscillators. The entire family of synchronization regions known as *Arnold tongues* might be represented in plots of coupling strength versus frequency or period mismatch. Although such stable states are expected in coupled systems of any nature, they can be predicted in oscillating coupled systems by means of some techniques such as Hilbert transform and Fourier analysis. However, a theoretical tool enabling a general prediction of synchronization of any order still remains unavailable.

Pulse-coupled oscillators have been extensively studied and used to model biological systems such as fireflies, crickets, and cardiac and neural cells. The study of how pulse-coupled oscillators achieve synchrony is relevant to the experimental observations of synchronous neural firing patterns in various mammalian, insect and reptilian species. Mirollo and Strogatz [22] proved that an ensemble of globally-coupled oscillators will synchronize under certain conditions.

From an analytical viewpoint, difficulties in the study of pulse-coupled oscillators are associated with the discontinuities introduced as a result of coupling. In particular, integrate-and-fire models are examples of this. Nevertheless, since the flexibility in the choice of parameter values leads to different forms of oscillation, most relaxation oscillators may be mimicked by light-controlled oscillators (LCOs). The analysis here is presented with the aim of depicting Arnold tongues and their stability for the simplest configuration. LCOs are one-dimensional relaxation oscillators described by two time-scales in a way that they mimic the synchronous behavior of some fireflies species [23,24]. As the discharging stage is related to the firing of the firefly, pulse-coupling forms can be accomplished using nearly null discharging time-scales. Nevertheless, as long as time-scales are properly defined, results presented here do not imply any constraints regarding the oscillating form of the LCO system.

Somers and Kopell [26] noted that synchronization occurs more rapidly in chains of relaxation oscillator when interactions occur in pulse-like form. Campbell and Wang [27] concluded that synchronization rates are also improved by coupling in the form of Heaviside step function, mainly due to the steepness of the interaction. Consistent results were obtained using LCOs [23,24].

In this paper, Arnold tongues were constructed for two coupled LCOs in Master-Slave (MS) configuration under

[a] e-mail: marti@fisica.edu.uy

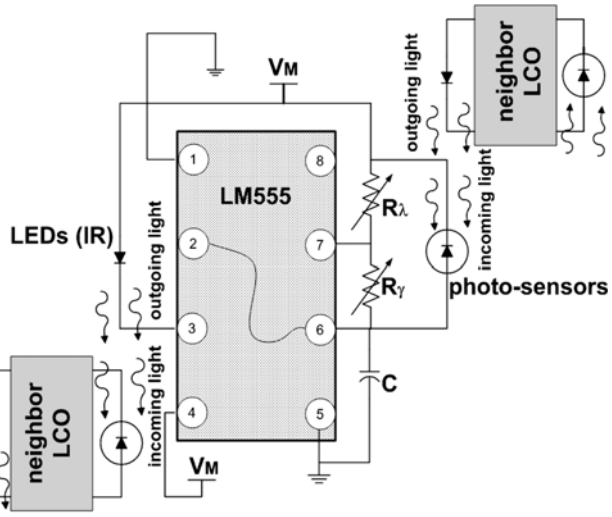

Fig. 1. Experimental scheme of an LCO coupled to other neighbour LCOs. LEDs and photodiodes enable the coupling among them.

varying period and coupling strength. This coupling configuration was studied experimentally and numerically for $(n : m)$ synchronization regions, whereas exact analytical results were possible only for $(1 : n)$ synchronous order, in which, the Arnold tongue shape and structure remain invariant varying n.

2 Light-controlled oscillators

The time-scale parameters of LCOs are chosen in a way that the resulting oscillating form resembled an integrate-and-fire model for the experimental observations, as this oscillating form results in smaller transients. Both time-scales may be modified manually on the spot, enabling quantitative measurement of phase differences and period variations within the required precision [23,24].

2.1 Experimental setup

Each LCO is composed of an LM555 chip operating in an astable oscillating mode and a dual RC sharing the capacitor (Fig. 1). The chip element selects the corresponding RC circuit, and sets sharp charging and discharging thresholds at $2V_{cc}/3$ and at $V_{cc}/3$, respectively, being V_{cc} the source voltage, which is approximately 9 V in this study. As it has been stated above, the associated charging and discharging times may be adjusted according to problem by modifying the resistors R_λ and R_γ connected in series with the LED, The duration of these stages are in the order of milliseconds. The period of each oscillator is determined by the sum of these durations.

Simple and cheap optoelectronic devices has been used in order to couple the LCOs. Each LCO is also composed of IR transmitter diodes (standard IR LEDs 3 mm Typ L-934f3bt) and commercial photodiodes (for instance, PD15-21C/TR8 SMD). LCOs can interact by means of light-pulses occurring during the discharging stage. Different degrees of coupling strength may be obtained by placing the oscillators at different distances or by electronically forcing greater emissions i.e. modifying the resistors connected to the LEDs. Previous work have shown that coupling strength varies roughly inversely as the square of the distance [23]. No time delays in the couplings were considered, in view of the characteristics of pulsed light. Differentially-masked sensors were used to achieve connectivity by directed coupling, enabling the study of the MS configuration. For further insights see references [23,24] and a detailed experimental setup of the LCOs is presented in [25]. The experimental measurements have been carried out using a Data Acquisition Card (NI-DAQ) that allowed us to obtain all the underlying dynamics of the system.

2.2 Model and state space

Based on the nature of the devices depicted in Figure 1 and their experimental behaviour, the LCOs are described by the following set of piecewise differential equations:

$$\dot{V}_i(t) = \lambda_i \left[V_{cc} - V_i(t)\right] \epsilon_i(t) - \gamma_i V_i(t) \left[1 - \epsilon_i(t)\right] + \sum_{j=1,\, j\neq i}^{N} \beta_{ij} \left[1 - \epsilon_j(t)\right],\ i = 1, \ldots, N, \quad (1)$$

where V_i is the ith LCO voltage, β_{ij} are the coefficients of the coupling matrix, and $\epsilon_i(t)$ is a binary variable representing the oscillator stage: $\epsilon = 1$, charging stage and $\epsilon = 0$, discharging stage. Thus, an LCO constitutes a one-dimensional oscillator. $\epsilon_i(t)$ changes its value when $V(t)$ reaches the upper threshold $(2V_{cc}/3)$ or the lower threshold $(V_{cc}/3)$. The parameters λ_i and γ_i are the characteristic charging and discharging frequencies, respectively. β_{ij} corresponds to a single element of the connectivity matrix which has zero diagonal elements. Equation (1) has been validated by several experimental results [23,24].

The solutions to equation (1) conform a continuous piecewise analytic flux that is naturally represented in the circle S^1 state space. The resultant state space can be thought to have an injective and a dissipative part of similar length. Through the injective part, the LCO charges over a time interval T_λ, whereas a fast discharge lasting T_γ occurs in the dissipative part. These time-scales are related to the characteristic frequencies of the LCOs λ and γ by

$$T_\lambda^{dark} = \ln(2)/\lambda, T_\gamma^{dark} = \ln(2)/\gamma, \quad (2)$$

whenever LCOs are masked, namely, *in dark*. The state space defined by the finite range of voltage amplitude $[V_{cc}/3, 2V_{cc}/3]$ constitutes an analogous situation. These thresholds are singular points where velocity changes sign and magnitude. This representation is useful for the construction of Lissajous figures.

Using the dimensionless variable $x_i(t) = [V_i(t) - V_{cc}]/(V_{cc}/3)$ for the ith oscillator, the corresponding

Table 1. Timescale sections of T^2 formed by two LCOs.

ϵ_1	ϵ_2	A_1	A_2	α_1	α_2
1	1	2	2	λ_1	λ_1
0	1	-1	$2+\tilde{\beta}_{21}/\lambda_2$	γ_1	λ_2
1	0	$2+\tilde{\beta}_{12}/\lambda_1$	-1	λ_1	γ_2
0	0	$\tilde{\beta}_{12}/\gamma_1-1$	$\tilde{\beta}_{21}/\gamma_2-1$	γ_1	γ_2

trajectories in state space for the two stages are:

$$x_i(t) = \left[x_i(t^*) - \left(\frac{\beta_{ij}/\lambda_i}{V_{cc}/3}[1-\epsilon_j(t)]+2\right)\right] e^{-\lambda_i(t-t^*)} + \left(\frac{\beta_{ij}/\lambda_i}{V_{cc}/3}[1-\epsilon_j(t)]+2\right), \quad (3)$$

for $\epsilon_i(t)=1$, and

$$x_i(t) = \left[x_i(t^*) - \left(\frac{\beta_{ij}/\gamma_i}{V_{cc}/3}[1-\epsilon_j(t)]-1\right)\right] e^{-\gamma_i(t-t^*)} + \left(\frac{\beta_{ij}/\gamma_i}{V_{cc}/3}[1-\epsilon_j(t)]-1\right), \quad (4)$$

for $\epsilon_i(t)=0$, where summation is done only where repeated j indexes occur and t^* represents the initial time condition in each stage. When an LCO reaches a threshold, $t \mapsto t^*$, and a new initial condition $x_i(t^*)$, $i=1,\ldots,N$ is generated for the global system.

As it can be seen from equation (4), the result of coupling is a rise in the asymptotic *in dark* level of the capacitor stages within the allowed thresholds. This corresponds to a displacement of the fixed points of equation (1) in the positive direction, which results in a faster charging stage and/or a slower discharging stage.

When dealing with two LCOs, some analytic results might be achieved. In particular, equation (4) takes the simple form:

$$x_i(t) = A_i + [x_i(t^*) - A_i]\, e^{-\alpha_i(t-t^*)}, \quad (5)$$

where each parameter can take the values shown in Table 1. MI configuration is achieved by setting $\tilde{\beta}_{ij} = \tilde{\beta}\ \forall i \neq j$ and MS corresponds to the case where $\tilde{\beta}_{12}=0$ if LCO_1 is used as master LCO ($\tilde{\beta}=\beta/V_{cc}/3$). This defines four sections onto the torus, each having a different timescale ratio. Sections are created according to the number of interacting LCOs. Thus, for N LCOs, the T^N torus has 2^N sections with different dynamics.

3 Synchronous stable states

Synchronization in LCOs is achieved once the period is locked. Depending on the frequency ratio of the oscillators, there are several locking possibilities. Synchronization is achieved as this ratio approaches a rational number. More generally [1], the condition is represented by the phase difference between oscillators

$$|\, n\,\Phi_i - m\,\Phi_j\,| < \epsilon_{(n:m)}. \quad (6)$$

This means that there is always a region where detuning between oscillators for a certain $(n:m)$ configuration results in a synchronous state.

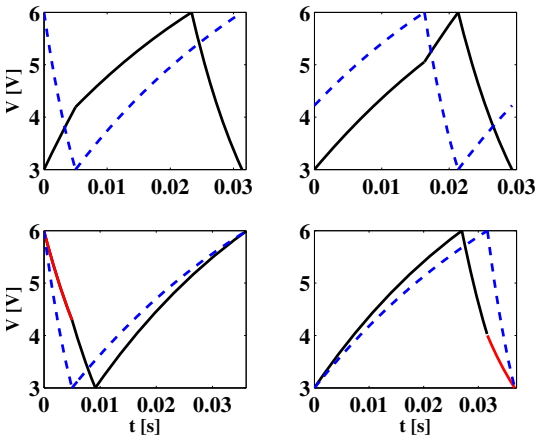

Fig. 2. (Color online) From left to right, equations (7)–(10). Four possible $(1:1)$ synchronous states. Master evolution is shown by the dashed line and Slave by the continuous line. Red lines indicate the modification on the shape of the Slave LCO discharging signal due to the action of the Master LCO. Time-scale parameters are: $T_{\gamma_S}=8$ ms, $T_{\gamma_M}=5$ ms and $T_{\lambda_S}=27$ ms.

3.1 MS Arnold tongues

Analytical results concerning synchronization regions in MS configuration can be achieved using the LCO model. In particular, four special situations for the $(1:n)$ state have simple analytical solutions. In these cases, analytical calculations are based on the states depicted in Figure 2. Whenever these situations prevail in time, meaning that coupling acts at a fixed position through the period of each Slave LCO, a synchronized state can occur. The evolution of the latter is constrained to have a period identical to that of the Master LCO. This figure shows two different special situations in both the charging and discharging stages. The edges of the synchronized state are those that become stable, as can be seen in Figure 3. The special states of coupled MS LCOs in the $(1:n)$ configuration are described by the following time-scale relations:

$$T_{\lambda_M}+T_{\gamma_M} = n\,(T_{\lambda_S}+T_{\gamma_S}) - \frac{1}{\lambda_S}\log\left[1+\frac{\beta/\lambda_S}{V_{cc}/3}\left(1-e^{-\lambda_S T_{\gamma_M}}\right)\right], \quad (7)$$

$$T_{\lambda_M}+T_{\gamma_M} = n\,(T_{\lambda_S}+T_{\gamma_S}) + \frac{1}{\lambda_S}\log\left[1+\frac{\beta/\lambda_S}{2V_{cc}/3}\left(1-e^{\lambda_S T_{\gamma_M}}\right)\right], \quad (8)$$

$$T_{\lambda_M}+T_{\gamma_M} = n\,(T_{\lambda_S}+T_{\gamma_S}) + \frac{1}{\gamma_S}\log\left[1+\frac{\beta/\gamma_S}{2V_{cc}/3}\left(e^{\gamma_S T_{\gamma_M}}-1\right)\right], \quad (9)$$

$$T_{\lambda_M}+T_{\gamma_M} = n\,(T_{\lambda_S}+T_{\gamma_S}) - \frac{1}{\gamma_S}\log\left[1+\frac{\beta/\gamma_S}{V_{cc}/3}\left(e^{-\gamma_S T_{\gamma_M}}-1\right)\right], \quad (10)$$

where, according to the plot on the top of Figure 3, equations (7) and (8) establish the interaction situations

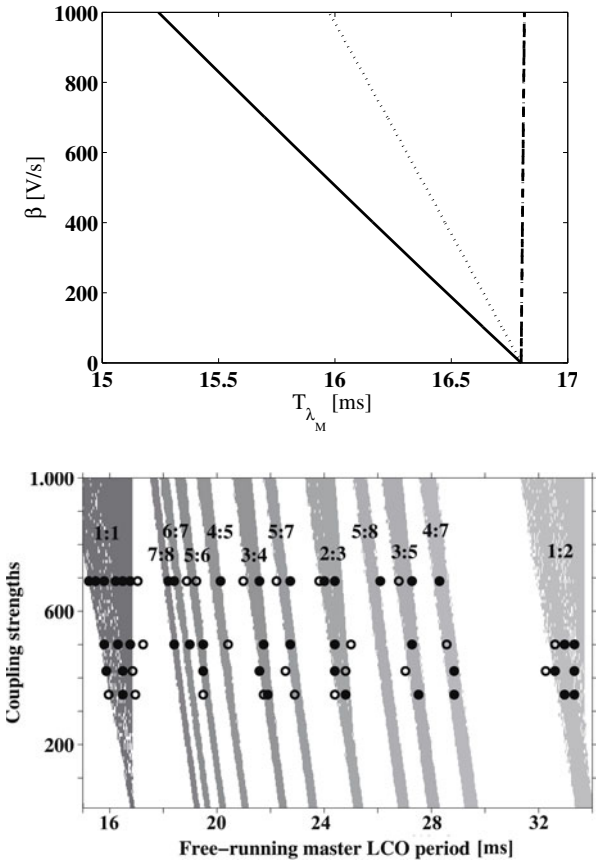

Fig. 3. On the top, analytically constructed Arnold tongue for (1 : 1) synchronization. From left to right, the different black lines correspond to equations (7)–(10) respectively, where equations (9)–(10) lead to an almost identical situation. On the bottom, the numerically obtained Arnold tongues are shaded and the experimental values are represented by circles. Filled circles correspond to stable states and open circles show phase-slip situations. The parameters are: $T_{\lambda_S} = 16.8$ ms and $T_{\gamma_S} = 0.2$ ms $= T_{\gamma_M}$.

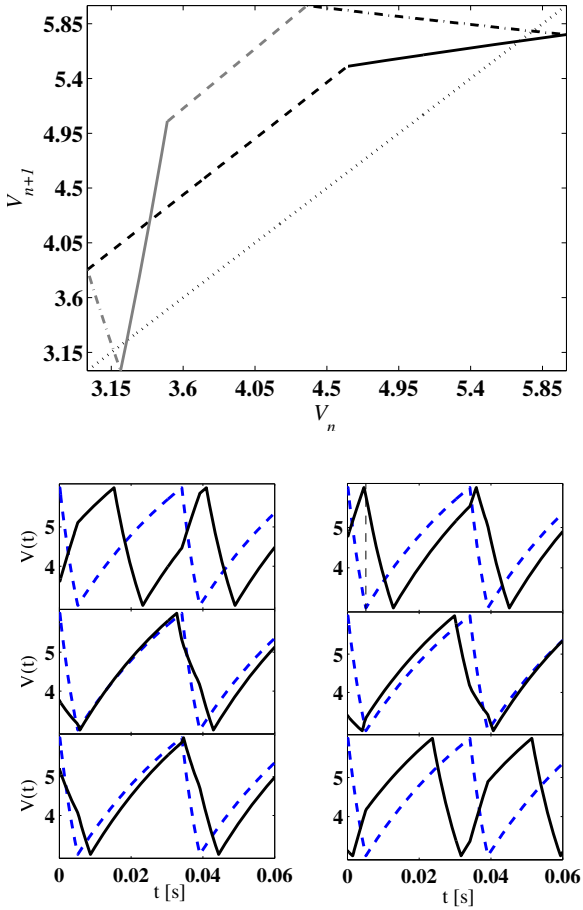

Fig. 4. (Color online) Top: return map for the MS configuration showing the stable fixed point (reference line crossing continuous black curve) and the unstable fixed point (reference line crossing the continuous gray curve). Bottom: six different flux evolutions corresponding to the different parts of the map. Dashed lines represent Master LCO evolution, while continuous lines represent Slave LCO evolution. Parameters were set at: $T_{\lambda_M} = 29$ ms, $\beta = 180$ V/s, in addition to those detailed in Figure 2.

during Slave LCO charge (left edges) and equations (9) and (10) the interaction situation during Slave LCO discharge (right edges); n is an integer corresponding to the $(1 : n)$ synchronized state, and the time-scales T_{λ_S}, T_{γ_S} and T_{γ_M} are the fixed *in dark* parameters. *In dark* T_{λ_M} was selected as control parameter. The resultant $(1 : n)$ Arnold tongue for $n = 1$ is shown on the left of Figure 3 where experimental values were used for the parameters.

Other synchronization regions verify transcendental analytical expressions, though numerical simulations could equally be used. This is particularly true when the Master LCO acts more than once over a single period of Slave LCO and there are not simple expressions of the control parameters as a function of the rest of the parameters involved.

The bottom plot in Figure 3 shows the experimental and numerical results found for several $(m : n)$ synchronous states as a function of *in dark* period detuning. Numerical simulations are based on a fourth order Runge-Kutta scheme that solves equation (1).

3.2 Stability windows

Within the (1 : 1) synchronization edges described by equations (7) and (10), an open stability window may be observed under all experimental conditions, as shown by the area comprised between the continuous and the dashed-dotted thick black lines in the top plot of Figure 3. In order to verify the stability within this region a complete return map was constructed according to:

$$V_{n+1} = V_{n+1}^{(S)} = f\left(V_n^{(S)}\right), \tag{11}$$

where V_n denotes the voltage of LCOs when the nth interaction starts.

As shown in Figure 4, it is possible to identify six regions on the map. Two branches (continuous and dashed thick black curves in the map of Fig. 4) reflect the

case where the Master LCO begins to act during Slave LCO charge ($\epsilon_M = 0, \epsilon_S = 1$) and represent the system evolving to the same situation. Other two branches correspond to the case where the Master LCO begins to act during Slave LCO discharge ($\epsilon_M = 0, \epsilon_S = 0$). Figure 4 shows these situations by the continuous and dashed thick gray lines. Each pair can be seen as two different maps, connected by the last two parts represented in this figure by black and gray dashed-dotted curves. These branches reflect that V_n with $\epsilon_M = 0$, $\epsilon_S = 1$ can evolve to V_{n+1} with $\epsilon_M = 0$, $\epsilon_S = 0$ and viceversa. In other words, to pass from the black to the gray line it is necessary to bounce on the negative slope curves of the map.

To illustrate the evolution features of the flux described by the map, Figure 4 (right) shows some examples. In the first row, the figures represent the dashed (continuous) thick black curves of the map, where the initial voltage was 3.6 V (4.7 V) in the left (right) columns. In the latter case, the system evolved from a situation where Master LCO starts acting from a point of the map during the charging stage through a point during the discharge of the Slave LCO, taking the latter to a similar situation. The following row in this figure corresponds to the dashed (continuous) gray curves, where initial voltages were 3.8 V (3.4 V). Under these initial conditions, both evolutions shifted from one branch of the map to the next one. Finally, the last row corresponds to initial voltages of 5.2 V (3.2 V). These plots describe the evolution of the system from the dashed-dotted black line to the continuous black line, and from the dashed-dotted gray line to the dashed black one, respectively.

In Figure 4 (left), it is possible to identify two fixed points: a stable (upper) one and an unstable (lower) one. The stable fixed point occurs (for properly defined β and T_{λ_M} values) in the region between equations (7) and (9) (also see Fig. 3). Within this region, the system achieves a synchronized state when Master LCO action begins during Slave LCO charge and ends during Slave LCO discharge. The unstable fixed point detaches the flux in two ways to achieve synchronization. In the region inside the Arnold tongue, near the left edge (Eq. (7)), there is no unstable fixed point, meaning that the system always achieves synchronization by increasing Master LCO action during Slave LCO discharge at these β and T_{λ_M} values.

For parameter values between equations (9) and (10), the former stable fixed point sinks and another fixed point arises in the dashed thick gray part of the map (as it can be seen in the map of Figure 5 for $\beta = 15$ V/s). This means that in the inner right part of the tongue, synchronization may be achieved by Master LCO action during Slave LCO discharge, retarding the latter. On the outer right edge (Eq. (10)), both the new stable point and the unstable point sink together.

These considerations can be seen in Figure 5, where all parameters are taken from Figure 2 and both T_{λ_M} and β are tuned. As an outstanding conclusion, we must point out that the stable solutions for any $(1 : n)$ synchronous regimes exhibit the same Arnold tongue shape

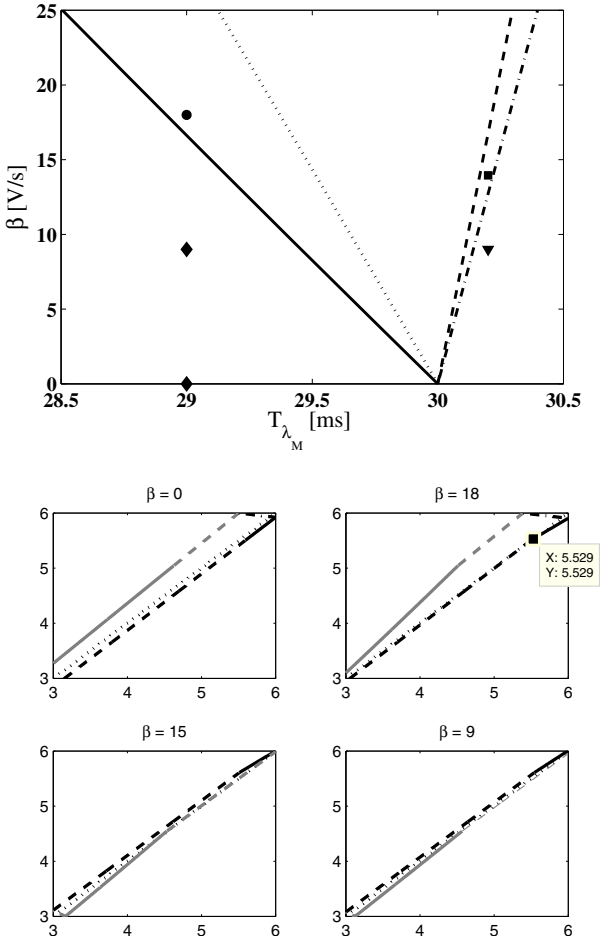

Fig. 5. On the top, analytical representation of the $(1 : 1)$ Arnold tongue, where parameters are as in Figure 2. On the bottom, four maps of the system evolution as coupling strength was tuned corresponding to this tongue. From left to right, the upper-row maps correspond respectively to the diamond and the circle shown in the left figure. The lower maps represent the evolution of the system in the right part of the tongue, which is shown in the left figure by a square and a triangle and for $\beta = 15$ V/s and $\beta = 9$ V/s respectively.

given by equations (7) and (10) with similar stability and constraints.

4 Final remarks

The dynamical model studied here is based on an electronic circuit. Analytical results are relevant for experimental guidance. In view of the simplicity of the model, conclusions regarding the synchronization properties of MS configurations as a function of fixed time-scale parameters are based on exact analytical results. Analytical expressions for $(1 : n)$ synchronization pose time-scale constraints and therefore synchronization restrictions for the MS system. From a counterintuitive view, these results showed that all $(1 : n)$ tongues have identical shape. Furthermore, because the analysis presented here applies

to any oscillating regime, the time-scale ratio need not be nearly zero as in the case of pulse-coupled oscillations or spiking regimes.

We observe that when the characteristic charging frequencies are smaller than discharging frequencies, $(1 : n)$ synchronization is achieved over a large range of the parameters, measured in terms of characteristic charging time of the Master LCO. This observation was verified by both experimental and numerical results. Results of stability analysis based on the first-return map of the Slave LCO were consistent with the above observations. The resultant $(1 : n)$ Arnold tongues for the MS configuration were found to remain invariant for all n, in both size and stability.

We acknowledge financial support from PEDECIBA, CSIC (U. de la República) and ANII (Uruguay). GMRA acknowledges J.L. Deneubourg and J.L. Guisset from the USE, ULB (Belgium) and the grant of the Deutscher Akademischer Austausch Dienst (Germany).

References

1. C. Schäfer, M.G. Rosenblum, H.H. Abel, J. Kurths, Phys. Rev. E **60**, 857 (1999)
2. A. Pikovsky, M. Rosenblum, J. Kurths, *Synchronization: A Universal Concept in Nonlinear Sciences* (Cambridge University Press, Cambridge, UK, 2001)
3. Edited by A. Pikovsky, Y. Maistrenko, *Synchronization: Theory and Application* (Kluwer Academic Publishers, Dordrecht, 2003)
4. S.C. Manrubia, A.S. Mikhailov, D.H. Zanette, *Emergence of Dynamical Order* (World Scientific Publishing, Singapore, 2004)
5. S.H. Strogatz, *Sync: The Emerging Science of Spontaneous Order* (Hyperion Press, NY, 2003)
6. V.Y. Argonov, S.V. Prants, Phys. Rev. A **71**, 053408 (2005)
7. W. Lauterborn, T. Kurz, U. Parlitz, Int. J. Bif. Chaos **7**, 2003 (1997)
8. J.C. Neu, SIAM J. Appl. Math. **38**, 305 (1980)
9. V. Astakhov, A. Shabunin, V. Demidov, A. Provata, F. Baras, G. Nicolis, V. Anishchenko, Chaos Solit. Fract. **15**, 395 (2003)
10. H. Fukuda, H. Morimura, S. Kai, Physica D **205**, 80 (2005)
11. B. Blasius, A. Huppert, L. Stone, Nature **399**, 354 (1999)
12. L. Glass, Nature **410**, 277 (2001)
13. D. Gonze, S. Bernard, C. Waltermann, A. Kramer, H. Herzel, Biophys. J. **89**, 120 (2005)
14. E. Despland, S.J. Simpson, Proc. R. Soc. B **273**, 1517 (2006)
15. L.O. Chua, J. Circ. Syst. Comp. **3**, 93 (1993)
16. K. Murali, M. Lakshmanan, L.O. Chua, Int. J. Bif. Chaos **5**, 563 (1995)
17. A. Kittel, J. Parisi, K. Pyragas, Physica D **112**, 459 (1998)
18. J. Cosp, J. Madrenas, E. Alarcón, E. Vidal, G. Villar, IEEE Trans. Neural Netw. **15**, 1315 (2004)
19. P.A. Pisarchik, R. Jaimes-Reátegui, J.H. García-López, Int. J. Bif. Chaos **18**, 1801 (2008)
20. N.F. Rulkov, Phys. Rev. Lett. **86**, 183 (2001)
21. N.F. Rulkov, Phys. Rev. E **65**, 041922 (2002)
22. R.E. Mirollo, S.H. Strogatz, SIAM J. App. Math. **50**, 1645 (1990)
23. G.M. Ramírez Ávila, J.L. Guisset, J.L. Deneubourg, Physica D **182**, 254 (2003)
24. N. Rubido, C. Cabeza, A.C. Martí, G.M. Ramírez Ávila, Phil. Trans. Royal Soc. A **367**, 3267 (2009)
25. J.L. Guisset, J.L. Deneubourg, G.M. Ramírez Ávila (2002), eprint `arXiv:nlin/0206036v1`
26. D. Somers, N. Kopell, Biol. Cybern. **68**, 393 (1993)
27. S.R. Campbell, D. Wang, C. Jayaprakash, IEEE Trans. Neural Netw. **15**, 1027 (2004)